Journal of Power Sources 247 (2014) 134–141

Contents lists available at ScienceDirect

Journal of Power Sources

journal homepage: www.elsevier.com/locate/jpowsour

Free-standing and mechanically flexible mats consisting of electrospun carbon nanofibers made from a natural product of alkali lignin as binder-free electrodes for high-performance supercapacitors

Chuilin Lai [a], Zhengping Zhou [b], Lifeng Zhang [c,*], Xiaoxu Wang [a], Qixin Zhou [b], Yong Zhao [a], Yechun Wang [b], Xiang-Fa Wu [b], Zhengtao Zhu [a], Hao Fong [a,**]

[a] Department of Chemistry and Applied Biological Sciences, South Dakota School of Mines and Technology, Rapid City, SD 57701, USA
[b] Department of Mechanical Engineering, North Dakota State University, Fargo, ND 58108, USA
[c] Joint School of Nanoscience and Nanoengineering, North Carolina Agricultural and Technical State University and the University of North Carolina at Greensboro, Greensboro, NC 27401, USA

HIGHLIGHTS

- Electrospun carbon nanofiber mats were made from a natural product of alkali lignin.
- The mats were free-standing and/or mechanically flexible.
- The mats had the BET specific surface area up to 583 $m^2\ g^{-1}$.
- The mats were studied as binder-free supercapacitor electrodes.
- Electrochemical performances of the electrodes were high.

ARTICLE INFO

Article history:
Received 22 May 2013
Received in revised form
11 August 2013
Accepted 20 August 2013
Available online 31 August 2013

Keywords:
Electrospinning
Carbon nanofiber
Supercapacitor
Alkali lignin

ABSTRACT

Mechanically flexible mats consisting of electrospun carbon nanofibers (ECNFs) were prepared by first electrospinning aqueous mixtures containing a natural product of alkali lignin together with polyvinyl alcohol (PVA) into composite nanofiber mats followed by stabilization in air and carbonization in an inert environment. Morphological and structural properties, as well as specific surface area, total pore volume, average pore size, and pore size distribution, of the lignin-based ECNF mats were characterized; and their electrochemical performances (*i.e.*, capacitive behaviors) were evaluated by cyclic voltammetry, galvanostatic charge/discharge, and electrochemical impedance spectroscopy. The lignin-based ECNF mats exhibited outstanding performance as free-standing and/or binder-free electrodes of supercapacitors. For example, the ECNFs made from the composite nanofibers with mass ratio of lignin/PVA being 70/30 (*i.e.*, ECNFs (70/30)) had the average diameter of ~100 nm and the Brunauer–Emmett–Teller (BET) specific surface area of ~583 $m^2\ g^{-1}$. The gravimetric capacitance of ECNFs (70/30) electrode in 6 M KOH aqueous electrolyte exhibited 64 F g^{-1} at current density of 400 mA g^{-1} and 50 F g^{-1} at 2000 mA g^{-1}. The ECNFs (70/30) electrode also exhibited excellent cycling durability/stability, and the gravimetric capacitance merely reduced by ~10% after 6000 cycles of charge/discharge.

1. Introduction

The storage of electrical energy has attracted growing interests particularly due to the fast-expanding markets of electric vehicles and portable electronic devices. In the recent years, electrochemical capacitors have been extensively investigated because of their high energy and power densities, rapid charge/discharge rates, and superior cycling durability [1,2]. In general, there are two types of electrochemical capacitors including supercapacitors (also known as electric double layer capacitors or ultracapacitors) and pseudocapacitors. Supercapacitors are able to store and release electrical energy through ion adsorption and desorption on electrode surface, and their capacitance is proportional to the specific surface area of their electrodes; while pseudocapacitors are capable of achieving energy storage and retrieval by charge transfer at the interface between electrode and electrolyte *via* reversible redox or Faradaic reactions.

Supercapacitors have been demonstrated to be useful for the applications such as memory backup system, auxiliary power unit,

* Corresponding author. Tel.: +1 336 285 2875; fax: +1 336 500 0115.
** Corresponding author. Tel.: +1 605 394 1229; fax: +1 605 394 1232.
E-mail addresses: lzhang@ncat.edu (L. Zhang), Hao.Fong@sdsmt.edu (H. Fong).

0378-7753/$ – see front matter © 2013 Elsevier B.V. All rights reserved.
http://dx.doi.org/10.1016/j.jpowsour.2013.08.082

instantaneous electricity compensator, and other energy-storage devices [3,4]. It is known that the efficiency and practicality of supercapacitors are primarily dependent upon electrode materials. Up to date, a variety of carbon-based electrode materials have been studied, for examples, activated carbons, carbon nanotubes [5], carbon nanofibers [6], carbon aerogels [7], carbide-derived carbons [8], and composite materials containing metal oxides [9] and graphene sheets [10,11]; among which, activated carbons are the most commonly adopted materials owing to their cost-effectiveness and high cycling durability [12]. However, organic/polymeric materials are typically required for binding the particles/powders of activated carbons to prepare the free-standing electrodes; whereas such binders would reduce the overall performance of electrodes. Hence, it is still a technological challenge to develop mechanically flexible electrodes with superior electrochemical performance, albeit numerous research efforts have been devoted to the fabrication of free-standing carbon-based electrode materials with high performance in the recent years.

Overlaid mats consisting of electrospun carbon nanofibers (ECNFs) can be prepared by electrospinning a spin dope (*e.g.*, a solution of polyacrylonitrile in *N*,*N*-dimethylformamide) into precursor nanofibers followed by the thermal treatments of stabilization and carbonization. These ECNF mats are mechanically resilient with relatively large specific surface areas; and thus they can be used directly as free-standing electrodes without addition of any binders. Previously reported studies have indicated that the ECNF mats could be promising for the fabrication of binder-free supercapacitors with high performance [8,13,14].

The development of carbon-based electrode materials from inexpensive, abundant, and sustainable natural sources has been paid more and more attentions among scientists worldwide; for examples, polypyrrole-cladophora cellulose composite paper [15], seaweed biopolymer [16], as well as cellulose, potato starch, and eucalyptus wood [17,18] have been recently studied as precursors to prepare carbon-based electrode materials for the fabrication of high-performance supercapacitors. Lignin is the second most abundant natural polymer after cellulose, and it is one of the most important renewable sources on earth. The molecules of lignin contain many aromatic components, making it suitable as carbon precursor. Lignin has been generated in large quantity as a by-product in pulping industry, in which three-dimensional (3-D) network of lignin in wood is disrupted and separated from cellulose fibers through the delignification process. Note that lignin has to be removed before wood pulp is turned into high-quality paper, and thus more than 15 million tons of lignin waste is generated each year in the United States alone. Different pulping techniques yield different types of lignin. One type is termed as Alcell lignin, which contains only a small amount of inorganic impurities. The major type of lignin is termed as alkali lignin (also known as Kraft lignin), which is generated from the Kraft pulping process. Unlike Alcell lignin, alkali lignin contains a relatively large amount of ashes and/or salts. Most alkali lignin is burned in the Kraft pulping process to produce energy for the recovery of pulping chemicals [19]. In the last several years, progresses have been made to prepare ECNFs from Alcell lignin [20,21]; and attempts have been successful in fabrication of porous carbon-based materials from alkali lignin [22,23]. Nevertheless, there have been no reported studies on (1) preparation of ECNF mats from alkali lignin and (2) fabrication and evaluation of supercapacitors with electrodes being such ECNF mats.

In this research, the mechanically flexible ECNF mats were prepared by electrospinning aqueous mixtures of alkali lignin and polyvinyl alcohol (PVA) into composite nanofiber mats first; and this was followed by stabilization and carbonization of the precursor mats in air and in an inert environment, respectively. Morphological and structural properties, as well as specific surface area, total pore volume, average pore size, and pore size distribution, of the lignin-based ECNF mats were characterized by scanning electron microscopy (SEM), transmission electron microscopy (TEM), and nitrogen sorption measurements, respectively; and the electrochemical performance (*i.e.*, capacitive behavior) was studied by cyclic voltammetry (CV), galvanostatic charge/discharge, and electrochemical impedance spectroscopy (EIS). The alkali lignin-based ECNF mats exhibited outstanding performance as free-standing/binder-free electrodes of supercapacitors. For comparison, the ECNF mats made from neat PVA were also prepared and studied. Furthermore, discussions on experimental results and the electrochemical mechanisms are given, and conclusions on the research are drawn consequently.

2. Materials and methods

2.1. Materials

The powder of alkali lignin was purchased from Sigma–Aldrich (catalog number 471003), it had the weight average molecular weight of 10,000 and contained 4 wt.% sulfur; this alkali lignin is also known as Kraft lignin and has a low content of sulfur. Poly (vinyl alcohol) (PVA) powder was also purchased from Sigma–Aldrich with molecular weight ranging from 85,000 to 124,000 and degree of hydrolysis of 87–89%. Both powders of alkali lignin and PVA were used as received without further purification. Unless otherwise noted, all of "lignin" appeared in the following text refers to alkali lignin, and all of percentages reported are weight percentages.

2.2. Electrospinning

To prepare the spin dopes with mass ratios of lignin/PVA being 30/70, 50/50, and 70/30, the lignin was first dispersed in an appropriate amount of distilled water, and the corresponding amounts of PVA were then added into each lignin aqueous mixture at 75 °C under constant stirring. Thereafter, each spin dope was loaded into a 30 mL BD Luer-Lok™ plastic syringe having a stainless-steel needle with 90° blunt end and innerdiameter of 0.4 mm. The electrospinning setup consisted of an ES30P high voltage DC power supply, purchased from the Gamma High Voltage Research, Inc. (Ormond Beach, FL), and a laboratory-produced roller with the diameter of 25 cm. The roller was placed at 25 cm from the tip of needle. During electrospinning, a positive voltage of 26 kV was applied to the needle, and the feeding rate of spin dope was maintained at 1.2 mL h^{-1} by using a KDS-200 syringe pump purchased from the KD Scientific Inc. (Holliston, MA). The lignin/PVA composite nanofibers were collected as overlaid mat on the electrically grounded aluminum foil that covered the roller. The lignin/PVA nanofiber mats were finally peeled off (from the aluminum foil) and stored in a desiccator before the subsequent stabilization and carbonization.

2.3. Stabilization and carbonization

To convert lignin/PVA composite nanofibers into carbon nanofibers, stabilization in air is necessary [24,25]. Prior to stabilization, the lignin/PVA nanofiber mats were wrapped onto a stainless steel rod. Stabilization was conducted in a Lindberg 54453 heavy duty tube furnace purchased from the TPS Co. (Watertwon, WI) with the following heating procedure: (1) temperature was increased from 25 to 100 °C at 10 °C min^{-1}; (2) temperature was held at 100 °C for 2 h; (3) temperature was increased from 100 to 180 °C at 1 °C min^{-1}; (4) temperature was held at 180 °C for 16 h; (5) temperature was increased from 180 to 220 °C at 0.5 °C min^{-1}; (6) temperature was held at 220 °C for 8 h; and (7) sample was cooled down to room temperature. A constant air flow was maintained

through the tube during the stabilization. The stabilized nanofiber mats were then un-wrapped from the stainless steel rod for the subsequent carbonization, and the following was the heating procedure: (1) temperature was increased from 25 to 1200 °C at 5 °C min^{-1}; (2) temperature was held at 1200 °C for 1 h; and (3) sample was cooled down to room temperature. A constant argon flow was maintained through the tube during the carbonization.

2.4. Characterization and evaluation

A Zeiss Supra 40VP field-emission scanning electron microscope (SEM) was employed to examine the morphologies of nanofiber mats. The average fiber diameter of each sample was determined by measuring diameters of 50 randomly selected nanofibers in the corresponding SEM image using the Image J software. The microstructures of carbon nanofiber mats were also investigated by transmission electron microscopy (TEM, Hitachi H-7000 FA quipped with a Kevex energy-dispersive X-ray spectrometer). The TEM specimens were prepared by dispersing the carbon nanofibers in ethanol followed by dropping the nanofiber-containing suspension over the copper grids with lacey carbon film. X-ray diffraction (XRD) patterns were acquired from a Rigaku Ultima Plus X-ray diffractometer operated at 40 kV and 90 mA with the CuKα radiation (wavelength $\lambda = 1.54$ Å). Raman spectra were acquired from a Nicolet NXR 9650 FT-Raman spectrometer, and the wavelength of source laser was 632.8 nm. Brunauer–Emmett–Teller (BET) specific surface area, total pore volume, average pore size, and pore size distribution were determined by N_2 adsorption at −196 °C with Micromeritics Analytical Services (Norcross, GA).

A symmetrical two-electrode cell was assembled as prototype supercapacitor using ECNF mats as electrodes (size ~ 1.0 cm^2). Two pieces of nickel–copper wire sheet were used as current collectors. Note that the ECNF mats were used without addition of any polymeric binder and/or conductive additive; *i.e.*, two ECNF mats were used to wrap the current collector and pressed securely to ensure good contact. The mass of ECNF mats was measured with an electronic balance (analytical grade). Electrochemical characterizations including cyclic voltammetry (CV), galvanostatic charge/discharge, and electrochemical impedance spectroscopy (EIS) of the ECNF electrodes were carried out by using the two-electrode cell in 6 M KOH aqueous solution with a supercapacitor tester (BT 2000, Arbin Instruments, TX) and an Electrochemical Multiplexer ECM8 (Gamry Instruments, Inc., PA). CV studies were performed at the scanning rates in the range from 5 to 2000 mV s^{-1} within the voltage window from 0 to 0.8 V. EIS measurements were carried out using the frequency range from 0.01 to 100 kHz.

3. Results and discussion

3.1. Morphological and structural properties

Due to lack of chain structures and/or molecular entanglements, an aqueous mixture containing alkali lignin alone could not be electrospun into nanofibers at any lignin concentration. In contrast, uniform PVA nanofibers with diameters of ~300 nm could be readily electrospun from 12 wt.% PVA aqueous solution. By electrospinning 9–12 wt.% aqueous mixtures containing both lignin and PVA (with different lignin/PVA weight ratios of 30/70, 50/50, and 70/30), the composite nanofibers of lignin/PVA with varied compositions could be prepared. SEM results revealed that the average diameters of composite nanofibers decreased with increasing the lignin amount from ~220 nm at 30 wt.% lignin, to ~170 nm at 50 wt.% lignin, and to ~140 nm at 70 wt.% lignin. It was intriguing that the average diameter of composite nanofibers (with the lignin/PVA weight ratio of 70/30) was less than a half of that of neat PVA nanofibers under the same electrospinning conditions (Fig. 1). This might be due to the decreased viscosity and increased conductivity of a spin dope when PVA was partially replaced by lignin. The decrease of viscosity was attributed to smaller molecular weight/size of lignin, while the increase of conductivity was

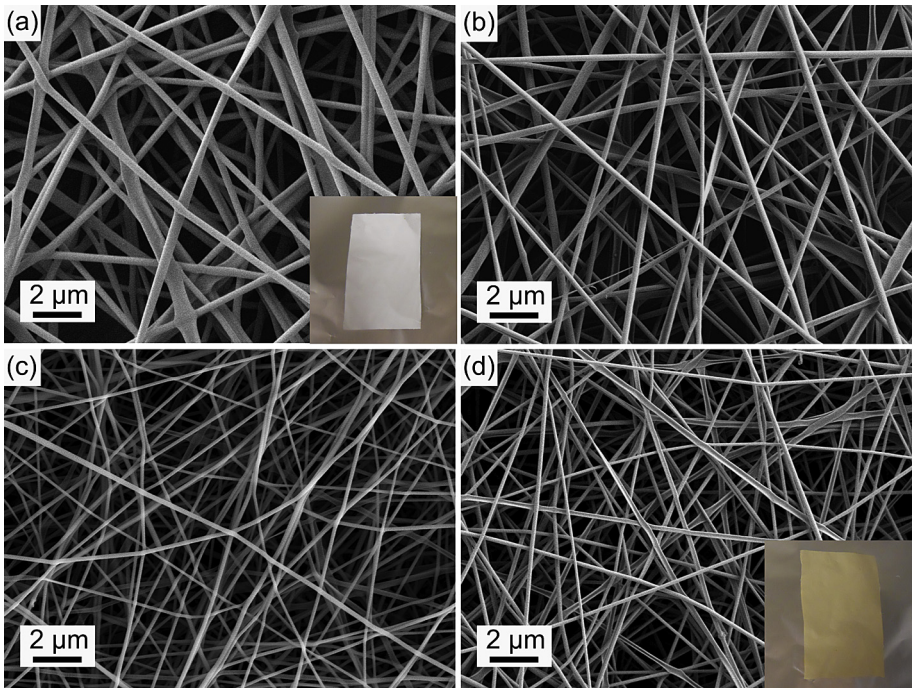

Fig. 1. SEM images of electrospun nanofiber mats: (a) neat PVA nanofiber mat from 12 wt.% aqueous solution; (b) 30/70 lignin/PVA composite nanofiber mat from 10 wt.% aqueous solution; (c) 50/50 lignin/PVA composite nanofiber mat from 9 wt.% aqueous solution; (d) 70/30 lignin/PVA composite nanofiber mat from 12 wt.% aqueous solution. The insets in images (a) and (d) depict the corresponding optical photos of mats (with sizes of ~2.5–5 cm).

attributed to higher content of inorganic salts in lignin. With the increase of lignin amount in spin dope, more fibers with the ribbon-shaped morphology was produced, suggesting that a spin dope with high lignin amount had the tendency to form thin and tube-like jet/filament during electrospinning, which could further collapse with the rapid vaporization of solvent [26,27]. As shown in the insets of Fig. 1(a) and (d), the color of neat PVA nanofiber mat was white, while the color of 70/30 lignin/PVA composite nanofiber mat was yellow. This was simply because the color of lignin powder was brown; hence, with the higher amount of lignin in composite nanofibers, the color of mat became darker.

After the thermal treatments of stabilization and carbonization, all of the resulting carbon nanofibers well-retained the overall morphologies of their precursor nanofibers. The average diameters of ECNFs, however, were much smaller than those of the precursor nanofibers. The average diameter of ECNFs made from neat PVA nanofibers was ~210 nm, while the average diameters of ECNFs made from lignin/PVA composite nanofibers with 30, 50, and 70 wt.% lignin were ~150, ~130, and ~100 nm, respectively. Because of removal of hydrogen, oxygen, and sulfur atoms, the carbonization process of lignin led to the significant reduction in fiber diameter and the formation of 3-D carbonaceous structures. Compared to the ECNFs made from Alcell lignin with diameters ranging from 400 nm to 1 μm [20], the ECNFs made from alkali lignin appeared to be much thinner. Note that the ECNFs (70/30) mat (made from composite nanofiber mat containing the highest amount of lignin) was mechanical flexibility, and it could be bent without breaking (see the inset in Fig. 2d); whereas the ECNFs (PVA) mat was brittle (see the inset in Fig. 2a).

Fig. 3 shows the high-resolution TEM images of different ECNFs, and the results are consistent with those acquired from SEM. In general, the ECNFs made from electrospun neat PVA and 30/70 lignin/PVA nanofibers had relatively smooth surfaces, while the other two ECNFs made from electrospun 50/50 and 70/30 lignin/PVA nanofibers had rough surfaces. The electron diffraction patterns (insets in Fig. 3) indicated that all of the ECNFs possessed the turbostratic graphitic microstructures, while there was no appreciable structural variation with the increase of lignin amount in the precursor nanofibers.

XRD analysis and Raman spectroscopy were also carried out to further characterize the microstructures of the prepared ECNFs. As shown in Fig. 4a, a broad diffraction peak was observed for all of ECNFs at the 2θ angles between 20° and 30°, which was attributed to the crystallographic plane of (002) in graphitic structure; and the broad peak indicated that the size of graphite crystallites might be small and the degree of graphitic order might be relatively low [28]. The two weak diffraction peaks centered at the 2θ angles of 44° and 51° were attributed to the crystallographic planes of (100) and (004) in graphitic structure, respectively. The average interplanar spacing "d(002)", calculated by the Bragg equation, increased from 0.371 nm for ECNFs (PVA) to 0.374, 0.401, and 0.418 nm for ECNFs (30/70), ECNFs (50/50), and ECNFs (70/30), respectively. The increase of average interplanar spacing was concomitant with the decrease of density [29], suggesting that more porous structures were derived from carbonization of composite nanofibers with higher amount of lignin.

Raman spectra of the ECNFs had two characteristic bands around 1350 and 1580 cm^{-1} (Fig. 4b). The band centered at 1350 cm^{-1} is related to disordered carbonaceous structures and is commonly referred as "D-band"; while the band centered at 1580 cm^{-1} is related to ordered graphitic structures and is commonly referred as "G-band". The "D-band" could be resulted from the vibrations of carbon atoms with dangling bonds in crystal lattice (due to in-plane terminations of disordered graphite) or from defects in the curved graphene sheets [30]. The "G-band" could be associated with the sp^2 vibrations of ordered graphitic structures [31–34]. The intensity ratio of "D-band" to "G-band" ("I_D/I_G", known as the "R-value") indicates the degree of structural disorder in carbonaceous materials. The R-values of ECNFs increased monotonically from 0.99 to 1.08 as the lignin amount in the precursor nanofibers increased from 0 to 70 wt.%, suggesting that some ordered graphitic structures were converted to disordered carbonaceous structures with the increase

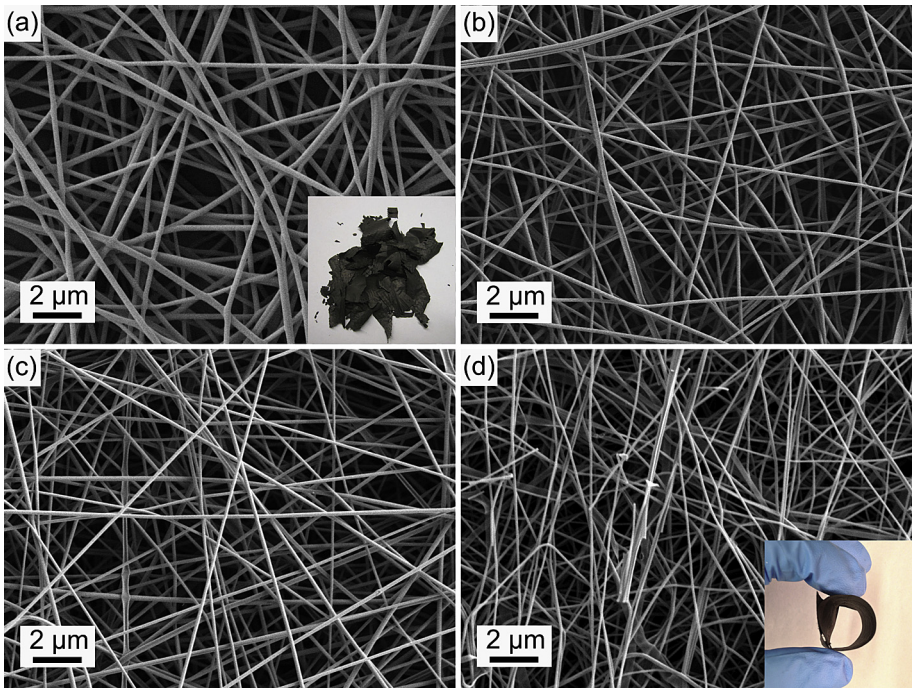

Fig. 2. SEM images of different ECNF mats: (a) ECNFs (PVA) mat, the inset showing that the mat was brittle; (b) ECNFs (30/70) mat, (c) ECNFs (50/50) mat, and (d) ECNFs (70/30) mat, the inset showing that the mat was flexible.

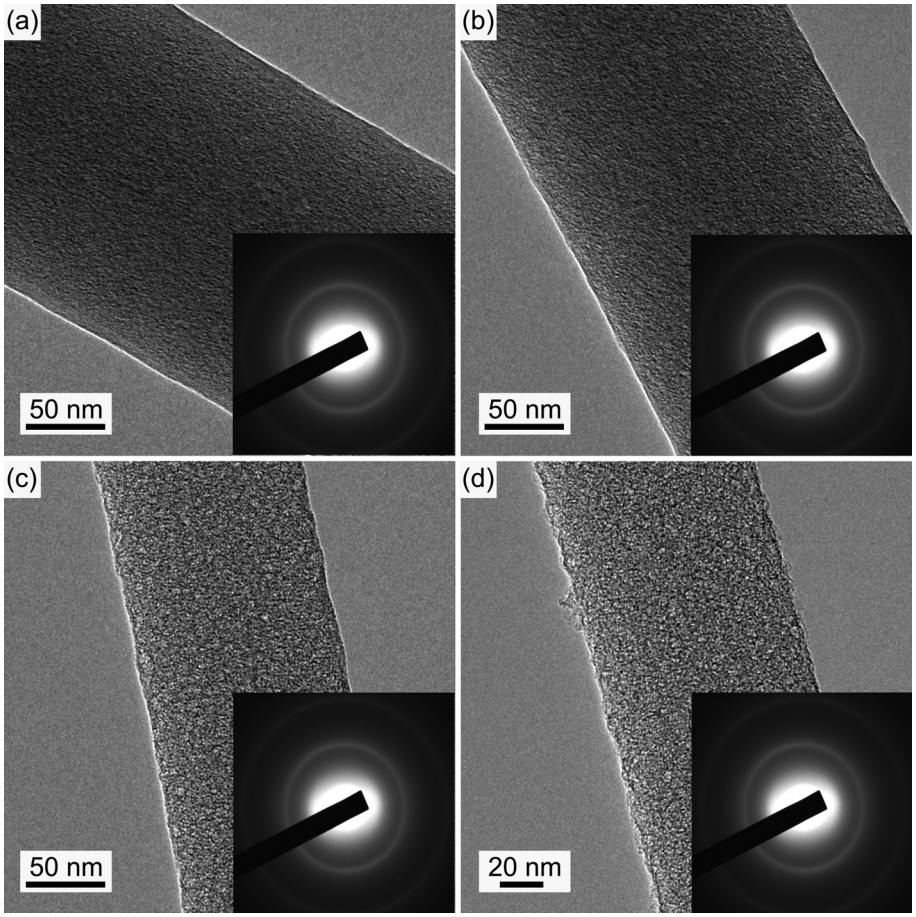

Fig. 3. TEM images and the corresponding electron diffraction patterns (insets) of (a) ECNF (PVA), (b) ECNF (30/70), (c) ECNF (50/50), and (d) ECNF (70/30).

of lignin amount in the precursor nanofibers. This observation was consistent with the TEM and XRD results.

N_2 adsorption was studied to measure the specific surface area, pore size distribution, average pore size, and pore volume of the prepared ECNFs (Fig. 5, Table 1). The N_2 adsorption plots in Fig. 5a can be classified as Type II under the Brunauer classification. The adsorption behavior includes adsorption in low pressure region ($P/P_0 < 0.1$), gradually increased adsorption in middle P/P_0 region, and further adsorption increase in high pressure region (>0.9 P/P_0), which were respectively ascribed to N_2 adsorption in micropores, mesopores, and multilayer adsorption of mesopores. Specific surface areas of the ECNFs were evaluated using the BET method. The ECNFs (PVA) had the lowest specific surface area of 14 m^2 g^{-1}, largest average pore size of 19.4 nm, and smallest pore volume of 0.022 cm^3 g^{-1}. With the increase of lignin amount in composite nanofibers, the specific surface area and pore volume of the resulting ECNFs increased while the average pore size decreased. The ECNFs (70/30) possessed the highly porous structure; compared to those of ECNFs (PVA), the specific surface area and total pore volume of ECNFs (70/30) substantially increased by more than 40 times to 583 m^2 g^{-1} and by more than 10 times to 0.289 m^3 g^{-1}, respectively, while the average pore size reduced significantly by 80% to 3.5 nm.

3.2. Electrochemical performance

Electrochemical capacitive performances of the prepared ECNFs were investigated by using cyclic voltammetry (CV), galvanostatic charge/discharge, and electrochemical impedance spectroscopy (EIS). Typical CV curves of ECNFs were acquired at the scan rate of 30 mV s^{-1} with the potential range of 0–0.8 V in 6 M KOH aqueous electrolyte (Fig. 6a). CV curves of the ECNFs made from the lignin/PVA composite nanofibers with higher amounts of lignin exhibited better quasi-rectangular shapes, indicating that these ECNFs would be more desired as electrode materials for the supercapacitor application. Among four ECNFs, the ECNFs (70/30) had the CV curve with the largest area of loop, suggesting the highest gravimetric capacitance. The sample of ECNFs (70/30) was further scanned at varied scan rates of 5–50 mV s^{-1} (Fig. 6b). With the increase of voltage sweep rate, the CV curves well-retained their quasi-rectangular shape, indicating a reversible supercapacitor behavior in 6 M KOH electrolyte within the potential range.

The method of galvanostatic charge/discharge was adopted to test the performance of electrochemical capacitors. The charge/discharge curves of different ECNF electrodes were obtained at a constant current density of 400 mA g^{-1} with the potential range of 0–0.8 V in 6 M KOH aqueous electrolyte (Fig. 6c). The charge/discharge curves of these ECNF electrodes (particularly that of the ECNFs (70/30) electrode) were approximately isosceles, suggesting the excellent capacitive performance (*e.g.*, great electrochemical stability and reversibility) [35]. The galvanostatic charge/discharge behavior of ECNFs (70/30) electrode was further studied at varied current densities of 400, 1000, and 2000 mA g^{-1} (Fig. 6d). These charge/discharge curves were almost linear, and the isosceles triangles indicated excellent supercapacitor behaviors.

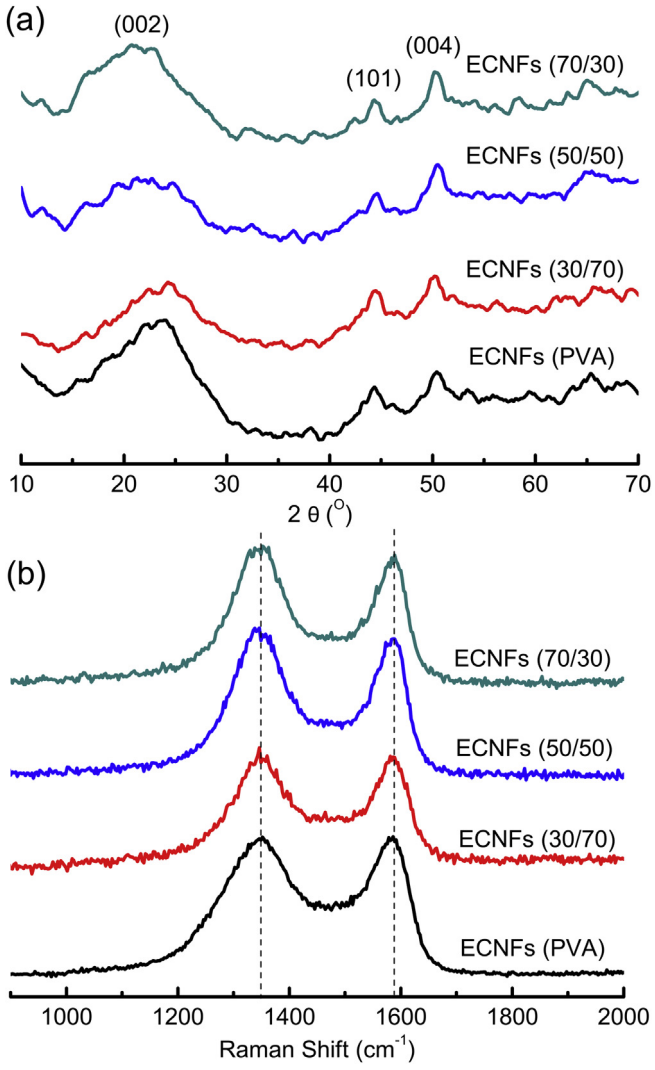

Fig. 4. XRD patterns (a) and Raman spectra (b) of different ECNFs.

The gravimetric capacitances of different ECNF electrodes were evaluated according to the following equation:

$$C = \frac{2 \times I \times \Delta t}{\Delta V \times m}$$

where I is the discharge current in ampere (A), ΔV is the potential difference during discharge in volt (V), Δt is the discharge time in the selected potential window in second (s), m is the mass of an electrode in gram (g), and C is the gravimetric capacitance (F g^{-1}). The gravimetric capacitances of ECNFs (PVA), ECNFs (30/70), ECNFs (50/50), and ECNFs (70/30) electrodes at the current density of 400 mA g^{-1} were determined at 10, 20, 32, and 64 F g^{-1}, respectively. The monotonic increase of gravimetric capacitance might be associated with the decrease of average pore size and the increase of specific surface area in the corresponding ECNFs as the lignin amount in precursor nanofibers increased. The gravimetric capacitances of the ECNFs (70/30) electrode at the current densities of 400, 1000, and 2000 mA g^{-1} were 64, 61, and 50 F g^{-1}, respectively. As the current density increased, the corresponding capacitance reduced slightly. It was observed that ~78% of the initial capacitance was retained at a relatively large current density of 2000 mA g^{-1} when ECNFs (70/30) was used as the electrode,

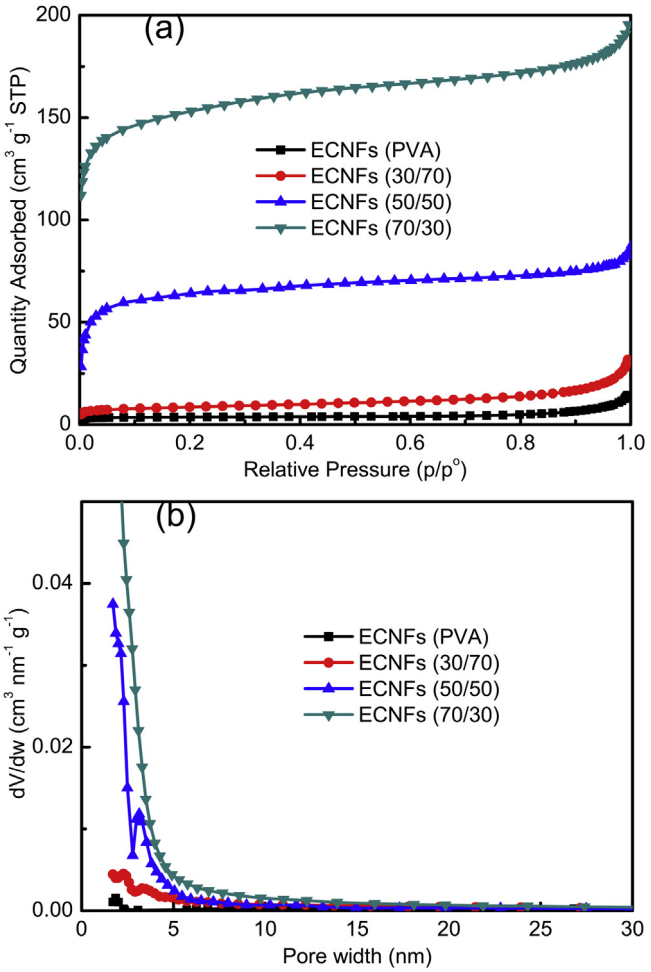

Fig. 5. N_2 adsorption isotherms (a) and pore size distributions (b) of different ECNFs. The pore size distribution was evaluated *via* the Barret–Joyner–Halenda (BJH) method.

suggesting that the ECNFs (70/30) mat/electrode could be suitable for the applications in which fast ion transportation and high current density would be required [36].

It is noteworthy that the ECNFs (70/30) electrode exhibited the gravimetric capacitance of 64 F g^{-1} at the current density of 400 mA g^{-1} in 6 M KOH aqueous electrolyte, which is similar to the electrode made of carbon nanotubes [1]; meantime, the energy density was 5.67 W h kg^{-1} and the power density was 94.19 W kg^{-1}. These results suggested that the ECNFs made from alkali lignin might be innovative carbon nanomaterials for energy storage applications.

EIS is a powerful technique to obtain the information on both the characteristics of pores and the dynamic ion diffusion in porous electrodes [37–39]. The complex-plane impedance plots (*i.e.*, the Nyquist plots) of ECNF electrodes showed depressed semi-circles at high frequency and straight lines nearly vertical to the realistic

Table 1
Values of the BET specific surface area (SSA), total pore volume, and average pore size acquired from N_2 adsorption isotherms at −196 °C for different ECNFs.

	BET SSA (m^2 g^{-1})	Total pore volume (cm^3 g^{-1})	Average pore size (nm)
ECNFs (PVA)	14	0.022	19.4
ECNFs (30/70)	31	0.049	8.9
ECNFs (50/50)	248	0.136	3.5
ECNFs (70/30)	583	0.289	3.5

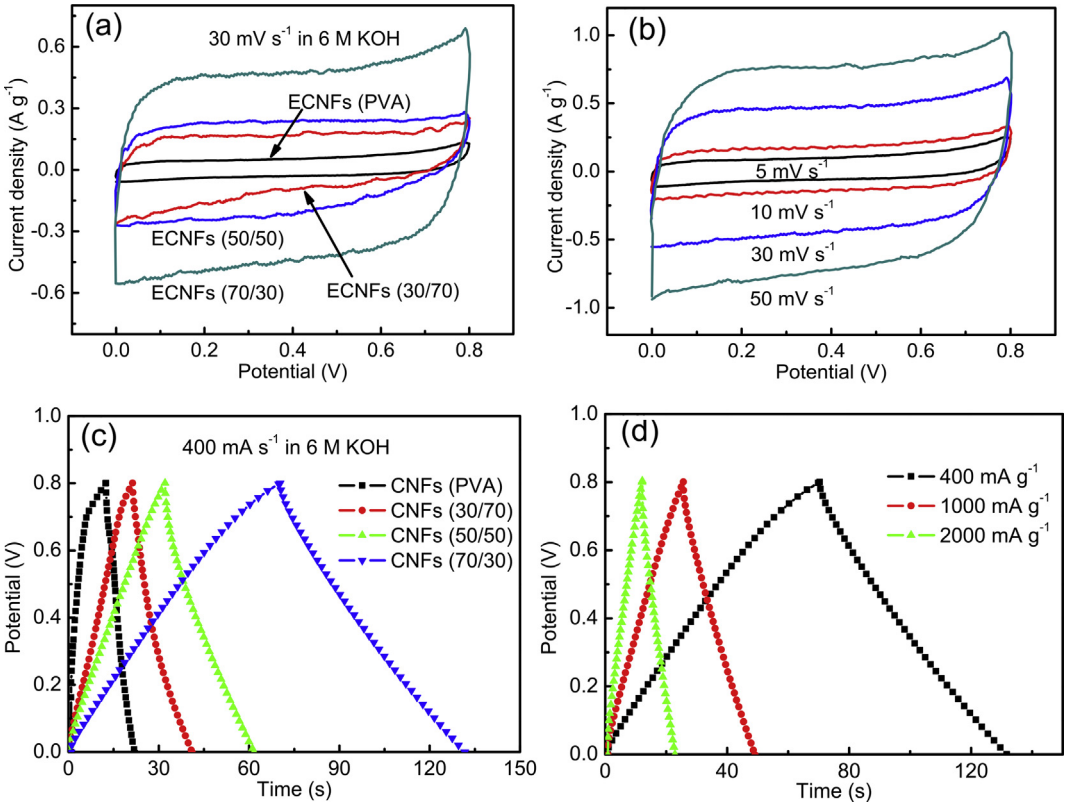

Fig. 6. Electrochemical characterizations of different ECNF electrodes in 6 M KOH aqueous electrolyte at room temperature: (a) cyclic voltammograms at the scan rate of 30 mV s^{-1} with the potential range of 0–0.8 V, (b) cyclic voltammograms of ECNFs (70/30) at varied scan rates, (c) galvanostatic charge/discharge curves at the current density of 400 mA g^{-1}, and (d) galvanostatic charge/discharge curves of ECNFs (70/30) at varied current densities.

impedance axis at low frequency, while no semi-circle was observed at high frequency on the plot of ECNFs (PVA). The diameter of those semi-circles increased with the increase of lignin amount in the precursor nanofibers. The Nyquist plots (Fig. 7) suggested that there were more cylindrical pores in ECNFs (PVA), while there were more turbination-shaped pores in ECNFs derived from lignin/PVA composite nanofibers [37]. Different diameters of the observed semi-circles also suggested that the ion adsorption efficiency was reduced with the increase of lignin amount in the composite nanofibers [38,39]. In general, the efficiency of ion diffusion would be reduced as the pore size became smaller. It is noteworthy that, although ECNFs (70/30) and ECNFs (50/50) had the similar average pore size based upon the results acquired from BET surface area analysis, these two mats/electrodes were quite different on their Nyquist curves, indicating ECNFs (70/30) might have smaller pores that ECNFs (50/50) did not possess.

The long cycling durability/stability is also a crucial parameter for electrode materials of supercapacitors. The stability of capacitance performance of the ECNFs (70/30) electrode was evaluated by employing the galvanostatic charge/discharge test for 6000 cycles between 0 and 0.8 V at a high constant current density of 2000 mA g^{-1} (Fig. 8). The gravimetric capacitance was merely reduced by approximately 10% after 6000 cycles of charge/discharge, indicating that the ECNFs (70/30) electrode was electrochemically stable/durable. The slight decrease of capacitance value with the increase of cycle number might be due to the loss of small amount of electrode materials, and this is common for carbonaceous materials with nano- and/or meso-porosities. Note that the performance of the 100th cycle appeared higher than that of the 1st cycle could be attributed to the wetting phenomenon, while the detailed mechanism(s) would be upon further investigations.

4. Conclusion

Mechanically flexible ECNF mats were prepared by electrospinning an aqueous mixture (containing a natural product of alkali

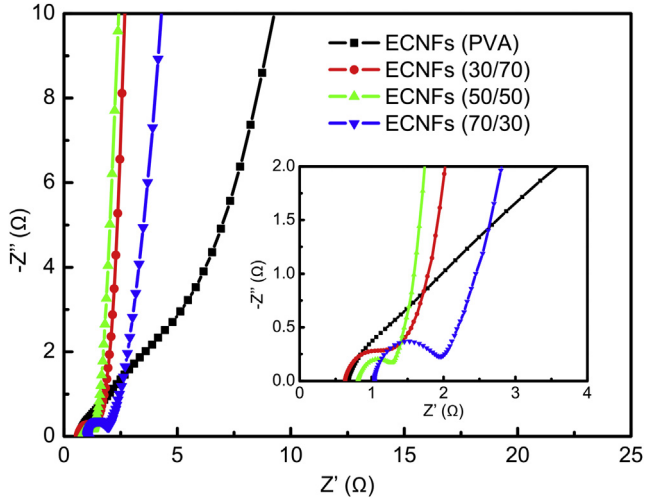

Fig. 7. Nyquist plots of different ECNF electrodes in 6 M KOH aqueous electrolyte. Z' and Z'' are the real and imaginary parts of the complex impedance Z, respectively. The inset is the magnified high-frequency region.

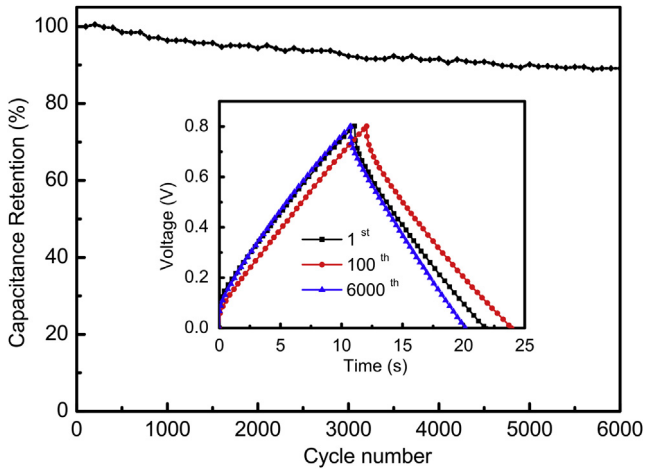

Fig. 8. Cycling stability of ECNFs (70/30) electrode at the current density of 2000 mA g^{-1}. The inset shows the charge/discharge curves of the 1st, 100th, and 6000th cycles at 2000 mA g^{-1}.

lignin together with PVA) into precursor nanofibers followed by stabilization in air and carbonization in Argon. The ECNF mats were studied as supercapacitor electrodes without addition of any binder. The ECNFs well-retained the overall morphologies of their precursors (*i.e.*, neat PVA nanofibers and lignin/PVA composite nanofibers), and showed ~30% reduction of fiber diameters. It was revealed that with the higher amount of lignin in the precursor nanofibers, the resulting ECNFs would have the smaller average pore size, larger pore volume, and higher specific surface area. The ECNFs (70/30), which was derived from the composite nanofibers with 70 wt.% lignin, had an average fiber diameter of ~100 nm and the BET specific surface area of 583 m^2 g^{-1}. The lignin-based ECNF mats (particularly the ECNFs (70/30) mats) demonstrated high performance as free-standing and/or binder-free electrode materials for supercapacitors. The ECNFs (70/30) mats had the highest gravimetric capacitance of 64 F g^{-1} at the current density of 400 mA g^{-1} and 50 F g^{-1} at 2000 mA g^{-1}; furthermore, the gravimetric capacitance was merely reduced by ~10% after 6000 cycles of charge/discharge, indicating that the ECNFs (70/30) electrode was electrochemically stable/durable. It is envisioned that the ECNF mats made from alkali lignin would be innovative and sustainable electrode materials for flexible high-performance supercapacitors.

Acknowledgments

This research was supported by the National Science Foundation (Grant No.: EPS-0903804), the National Aeronautics and Space Administration (Cooperative Agreement No.: NNX10AN34A), the Department of Energy (Award No.: DE-FG02-08ER64624), and the State of South Dakota.

References

[1] L.L. Zhang, X.S. Zhao, Chem. Soc. Rev. 38 (2009) 2520–2531.
[2] C.Z. Yuan, B. Gao, L.F. Shen, S.D. Yang, L. Hao, X.J. Lu, F. Zhang, L.J. Zhang, X.G. Zhang, Nanoscale 3 (2011) 529–545.
[3] X.Y. Chen, Q.Q. Zhou, Electrochim. Acta 71 (2012) 92–99.
[4] D. Pech, M. Brunet, H. Durou, P. Huang, V. Mochalin, Y. Gogotsi, P.L. Taberna, P. Simon, Nat. Nanotechnol. 5 (2010) 651–654.
[5] C. Emmenegger, P. Mauron, P. Sudan, P. Wenger, V. Hermann, R. Gallay, A. Zuttel, J. Power Sources 124 (2003) 321–329.
[6] E.J. Ra, E. Raymundo-pinero, Y.H. Lee, F. Beguin, Carbon 47 (2009) 2984–2992.
[7] C. Moreno-Castilla, M.B. Dawidziuk, F. Carrasco-Marin, Z. Zapata-Benabithe, Carbon 49 (2011) 3808–3819.
[8] V. Presser, L. Zhang, J.J. Niu, J. McDonough, C. Perez, H. Fong, Y. Gogotsi, Adv. Energy Mater. 1 (2011) 423–430.
[9] S.D. Perera, B. Patel, N. Nijem, K. Roodenko, O. Seitz, J.P. Ferraris, Y.J. Chabal, K.J. Balkus, Adv. Energy Mater. 1 (2011) 936–945.
[10] R.B. Rakhi, W. Chen, D. Cha, H.N. Alshareef, Adv. Energy Mater. 2 (2012) 381–389.
[11] X. Lu, H. Dou, B. Gao, C. Yuan, S. Yang, L. Hao, L. Shen, X. Zhang, Electrochim. Acta 56 (2011) 5115–5121.
[12] J. Gamby, P.L. Taberna, P. Simon, J.F. Fauvarque, M. Chesneau, J. Power Sources 101 (2001) 109–116.
[13] Y. Gao, V. Presser, L. Zhang, J.J. Niu, J.K. McDonough, C.R. Perez, H. Lin, H. Fong, Y. Gogotsi, J. Power Sources 201 (2012) 368–375.
[14] Z. Tai, X. Yan, J. Lang, Q. Xue, J. Power Sources 199 (2012) 373–378.
[15] A. Razaq, L. Nyholm, M. Sjodin, M. Stromme, A. Mihranyan, Adv. Energy Mater. 2 (2012) 445–454.
[16] E. Raymundo-pinero, F. Leroux, F. Beguin, Adv. Mater. 18 (2006) 1877–1882.
[17] H. Zhu, X. Wang, F. Yang, X. Yang, Adv. Mater. 23 (2011) 2745–2748.
[18] L. Wei, M. Sevilla, A.B. Fuertes, R. Mokaya, G. Ynshin, Adv. Energy Mater. 1 (2011) 356–361.
[19] S. Kubo, Y. Uraki, Y. Sano, Carbon 36 (1998) 1119–1124.
[20] M. Lallave, J. Bedia, R. Ruiz-Rosas, J. Rodriguez-Mirasol, T. Cordero, J.C. Otero, M. Marquez, A. Barrero, I.G. Loscertales, Adv. Mater. 19 (2007) 4292–4296.
[21] R. Ruiz-Rosas, J. Bedia, M. Lallave, I.G. Loscertales, A. Barrero, J. Rodriguez-Mirasol, T. Cordero, Carbon 48 (2010) 696–705.
[22] K. Babel, K. Jurewicz, Carbon 46 (2008) 1948–1956.
[23] M. Kijima, T. Hirukawa, T. Hata, Bioresour. Technol. 102 (2011) 6279–6285.
[24] S. Kubo, J.F. Kadla, J. Polym. Environ. 13 (2005) 97–105.
[25] J.L. Braun, K.M. Holtman, J.F. Kadla, Carbon 43 (2005) 385–394.
[26] C. Huang, S. Chen, C. Lai, D.H. Reneker, H. Qiu, Y. Ye, H. Hou, Nanotechnology 17 (2006) 1558–1563.
[27] S. Koombhongse, W. Liu, D.H. Reneker, J. Polym. Sci. Part B: Polym. Phys. 39 (2001) 2598–2606.
[28] Z. Zhou, K. Liu, C. Lai, L. Zhang, J. Li, H. Hou, D.H. Reneker, H. Fong, Polymer 51 (2010) 2360–2367.
[29] B.-J. Kim, S.-J. Park, J. Colloid Interface Sci. 315 (2007) 791–794.
[30] C.-W. Huang, C.-H. Hsu, P.-L. Kuo, C.-T. Hsieh, H. Teng, Carbon 49 (2011) 895–903.
[31] A.M. Rao, E. Richter, S. Bandow, B. Chase, P.C. Eklund, K.A. Williams, S. Fang, K.R. Subbaswamy, M. Menon, A. Thess, R.E. Smalley, G. Dresselhaus, M.S. Dresselhaus, Science 275 (1997) 187–191.
[32] C. Kim, S.-H. Park, J.-I. Cho, D.-Y. Lee, T.-J. Park, W.-J. Lee, K.-S. Yang, J. Raman Spectrosc. 35 (2004) 928–933.
[33] Z. Zhou, C. Lai, L. Zhang, Y. Qian, H. Hou, D.H. Reneker, H. Fong, Polymer 50 (2009) 2999–3006.
[34] H. Niu, J. Zhang, Z. Xie, X. Wang, T. Lin, Carbon 49 (2011) 2380–2388.
[35] W. Xing, C.C. Huang, S.P. Zhuo, X. Yuan, G.Q. Wang, D. Hulicova-Jurcakova, Z.F. Yan, G.Q. Lu, Carbon 47 (2009) 1715–1722.
[36] Y. Lv, L. Gan, M. Liu, W. Xiong, Z. Xue, D. Zhu, D.S. Wright, J. Power Sources 209 (2012) 152–157.
[37] H.-Q. Li, J.-Y. Luo, X.-F. Zhou, C.-Z. Yu, Y.-Y. Xia, J. Electrochem. Soc. 154 (2007) A731–A736.
[38] C.-L. Liu, W. Dong, G. Cao, J. Song, L. Liu, Y. Yang, J. Electrochem. Soc. 155 (2008) F1–F7.
[39] H. Lu, W. Dai, M. Zheng, N. Li, G. Ji, J. Cao, J. Power Sources 209 (2012) 243–250.